FASE FRONTIERS OF AGRICULTURAL SCIENCE AND ENGINEERING

Engineering Transactions of CAE

RESEARCH ARTICLE

2026 / Volume 13 / Issue 3 / 25666

Immune mechanism of oligochitosan-induced resistance toward potato virus Y in *Nicotiana benthamiana*

Shanxue ZHANG, Chunle WEI, Lu YU (✉), Baoan SONG (✉)

State Key Laboratory of Green Pesticide, Guizhou University, Guiyang 550025, China.

KEYWORDS

MAPK signaling pathway, oligochitosan, potato virus Y, reactive oxygen species

HIGHLIGHTS

- COS exhibits good anti-PVY activity.
- COS increases the activities of defense-related enzymes and the accumulation of ROS.
- COS promotes the expression of *OXI1*, *MAPKKK21*, and *NDPK4* in the MAPK pathway.

Received June 28, 2025;
Accepted September 9, 2025.

Correspondences: lyu1@gzu.edu.cn, basong@gzu.edu.cn

GRAPHICAL ABSTRACT

1. COS exhibits good anti-PVY activity and mainly mediates MAPK and ABA signal transduction.
2. OXI1 plays a positive regulatory role in the process of COS induced resistance to PVY.

ABSTRACT

This study investigated the antiviral activity and molecular mechanisms of oligochitosan against potato virus Y (PVY) in *Nicotiana benthamiana*. The results demonstrate that oligochitosan exhibits significant anti-PVY activity, achieving a preventive efficacy of 54.7%. Biochemical analyses revealed that oligochitosan treatment enhances the activities of defense-related enzymes and stimulates hydrogen peroxide accumulation in *N. benthamiana*. Integrated transcriptomic and proteomic analyses identified key differentially expressed genes associated with reactive oxygen species signaling and the mitogen-activated protein kinase pathway, including *PYL1*, *PP2C*, *OXI1*, *NDPK4*, *MAPKKK21* and *POD4*. Functional characterization demonstrated that oligochitosan specifically upregulates *OXI1* expression while enhancing *MAPKKK21* and *NDPK4* transcript levels, thereby conferring enhanced PVY resistance. These findings establish that oligochitosan-induced plant defense against PVY operates primarily through ROS-mediated activation of the mitogen-activated protein kinase signaling cascade. This work provides novel insights into the molecular basis of the antiviral activity of oligochitosan in plant protection.

1 Introduction

Through extensive research on the interactions between plants and pathogens, as well as plant immune responses, plant inducers that trigger disease resistance have become important new tools for managing crop diseases[1]. Studies show that oligochitosan (COS) is an effective and ecofriendly biological inducer, mainly produced by breaking down natural chitosan (CS) through biological, chemical or physical methods[2]. COS has remarkable bioactivity against a range of plant pathogens, including fungi, viruses and bacteria[3]. It has been proved to regulate stomatal closure in tobacco, induce reactive oxygen species (ROS) bursts, and influence plant signaling pathways such as salicylic acid and mitogen-activated protein kinase (MAPK), thereby enhancing plant disease resistance[4]. Nevertheless, the precise link between COS-induced ROS signaling and intracellular pathways like MAPK remains unclear. Also, previous studies on COS-induced disease resistance have largely focused on tobacco mosaic virus, with limited systematic investigation into the effects of COS and its mechanisms against potato virus Y (PVY), a highly destructive virus that causes significant yield losses in potatoes and tobacco crops in developing countries[5]. This gap has somewhat restricted the broader application of COS in controlling PVY.

Plant elicitors must be recognized through plant cell-to-cell interactions to transmit extracellular signals into the cells and activate downstream immune responses, thereby triggering plant disease resistance[6]. Previous studies have identified specific COS binding sites on the cell membranes of strawberries and tobacco plants, as well as three distinct COS receptor proteins, namely W5G2U8, W5HY42 and W5I0R4, on the wheat cell membranes[7]. Once the elicitor binds to the cell membrane receptor, it activates secondary signaling molecules, such as H_2O_2, which convey external signals into the cell and amplify them via the MAPK signaling pathway[8]. COS induces the outbreak of ROS in crop cells, including tobacco and strawberries, and influences MAPK signaling in crops such as tobacco and rice[9]. However, the exact connection between COS-induced ROS signaling and the MAPK pathway remains unclear.

ROS are essential signaling molecules that allow cells to rapidly respond to various stimuli, such as hydrogen peroxide and singlet oxygen ($^1O^2$)[10]. Fluctuations in ROS levels can alter the structure and function of numerous proteins, thereby affecting multiple signaling pathways. This is important in detecting stress, integrating diverse stress response signaling networks, and triggering and regulating plant defense mechanisms[10]. Within cells, ROS primarily influences signaling pathways through the posttranslational oxidative modification of OXI kinase[11]. The oxidative stress-inducible kinase 1 (OXI1) is a crucial plant protein that responds to oxidative signals and is essential for innate plant resistance to microbial pathogens as well as root hair development[12]. The *OXI1* gene, which encodes a serine/threonine kinase, is necessary for the full activation of *MPK3* and *MPK6* following ROS exposure, and studies have shown that H_2O_2 can stimulate its expression in *Arabidopsis*[13].

MAPK is a crucial signal transducer that conveys signals from the extracellular environment to the nucleus and can be activated by external factors such as hormones and cellular stress[14]. It is commonly found in eukaryotic cells and constitutes a highly conserved signaling pathway comprising MAPK, MAPK kinase (MEK), and MEK kinase (MEKK)[15]. This pathway operates through a sequential phosphorylation process, MEKK phosphorylates MEK, which then phosphorylates MAPK, thereby amplifying and relaying external signals in a cascade. The MAPK signaling pathway is a critical component in the growth, development and resistance of plants to external stress[16]. In plants, NDPKs are enzymes that are highly conserved, catalyzing the transfer of terminal phosphate groups from nucleoside triphosphates (NTPs) to nucleoside diphosphates (NDPs)[17]. They maintain the balance between intracellular NTPs and NDPs, and provide NTPs for biosynthesis, in addition to adenosine triphosphate[17]. Based on their amino acid sequences, plant NDPKs are classified into four distinct types (I-IV). NDPK I is mainly linked to plant growth and development, bacterial stress responses, abiotic stress and hormone signaling[18]. NDPK II is primarily involved in photosynthesis and ROS scavenging[19]. NDPK III is key in plant energy metabolism, programmed cell death and other functions[20]. NDPK IV gene is found only in the genomes of *Arabidopsis* and rice, and its role remains unclear. Of the NDPKs, only NDPK II is involved in ROS signal transduction and the regulation of oxidative stress[21].

Recent studies have shown that plant pattern-triggered immunity (PTI) and effector-triggered immunity (ETI), previously believed to be separate immune systems, actually collaborate to enhance plant immune responses[22]. Research has also demonstrated that COS can trigger early H_2O_2

production in plants and influence the MAPK signaling pathway, although the exact connection between these events is still not fully understood[9].

This study explores how COS improves tobacco resistance to PVY by using physiologic, biochemical and multi-omics approaches. Functional validation using RT-qPCR, Western blot and *OXI1* mutant assays confirmed its role in ROS-MAPK signaling. These findings clarify the antiviral mechanisms triggered by COS and support its application in managing PVY and enhancing plant immunity.

2 Materials and methods

2.1 Plant materials and chemicals

The materials were sourced from multiple places: the PVY virus from the Hunan Academy of Agricultural Sciences; PVY-GFP *Agrobacterium* from the Shandong Agricultural University, *Nicotiana benthamiana* from the Chinese Academy of Agricultural Sciences, *OXI1*-modified *N. benthamiana* strains from Wuhan Biorun Biotechnology (Figs. S1 and S2); and COS/CS from Hainan Zhengye Zhongnong High-tech.

2.2 Anti-PVY activity assays

Samples were dissolved in either 1% Tween-80 (COS), or a combination of 1% citric acid and 1% Tween-80 (CS) to create stock solutions at a concentration of 400 μg·mL^{-1}, which were then serially diluted to concentrations ranging from 200 to 25 μg·mL^{-1}. Three biological replicates of *N. benthamiana* plants at the four to six leaf stage were sprayed with the treatment solutions or a negative control (1% aqueous Tween-80 aqueous solution) applying 20 mL per treatment, with 10 plants per replicate. After 24 h, PVY-GFP (OD_{600} from 0.4 to 0.8) was infiltrated into the leaves using an *Agrobacterium*-mediated infiltration method. Plant phenotypes were recorded 14 days postinoculation, and PVY coat protein (PVY-CP) expression levels were measured by RT-qPCR using the TB Green Premix Ex *Taq*II kit (TaKaRa) and primers listed in Table S1. The cycling parameters were as follows: initial denaturation at 94 °C for 30 s; 40 cycles of 94 °C for 5 s, 45–60 °C for 30 s (optimized per primer), and 72 °C for 30 s; followed by a melt curve analysis of 95 °C for 15 s, 60 °C for 1 min, and 95 °C for 15 s. Expression levels were calculated using the $2^{-\Delta\Delta Ct}$ method, and protective efficacy (E) was determined as:

$$E = (A - B)/A \times 100\% \quad (1)$$

where, A represents PVY-CP expression in PVY-only samples and B represents PVY-CP expression in PVY samples treated with COS or CS.

2.3 Defense-related enzymes and H_2O_2 level assays

The activities of defense-related enzymes and H_2O_2 level were measured using previously established methods with some modifications[23]. *N. benthamiana* plants at the 4–6 leaf stage were divided into four treatment groups: CK, PVY, COS and PVY + COS. Each group included three replicates, with 10 plants per replicate. All leaves were sprayed with either 100 μg·mL^{-1} COS or a blank control solution for 24 h. Then, the lower three leaves were inoculated with PVY using the friction inoculation method. After inoculation, each plant was rinsed with deionized water, gently dried with blotting paper, and transferred to a greenhouse for growth under controlled conditions: 16:8 h L:D photoperiod, 26 °C and 70% relative humidity. Leaf samples were collected at 1, 3, 5 and 7 days postinoculation for omics analysis. The activities of catalase (CAT), superoxide dismutase (SOD), peroxidase (POD), and phenylalanine ammonia-lyase (PAL) were measured using commercial kits from Suzhou Comin Biotech, while H_2O_2 levels were determined using the Amplex Red kit from Invitrogen (Thermo Fisher, Waltham, MA, USA).

2.4 Transcriptome and proteome analysis

2.4.1 Treatment of plant samples

N. benthamiana plants with four to six leaves were arbitrarily assigned to two groups: PVY and PVY + COS, each consisting of three replicates with 20 plants per replicate. PVY + COS groupwas sprayed with a 100 μg·mL^{-1} solution of COS. After 24 h, plants were mechanically inoculated with PVYand then to a greenhouse maintained at 26 °C and 70% relative humidity growth.

2.4.2 Transcriptome analysis

Total RNA was extracted using a commercial kit (RNeasy, Qiagen, Inc., Chatsworth, CA, USA), and its concentration and purity were assessed with the Agilent 2100 Bioanalyzer (criteria: RNA concentration ⩾ 400 ng·μL^{-1}, OD_{260}/OD_{280}

ratio from 1.8 to 2.1, rRNA ratio (28S/18S) ⩾ 2.0 and RIN ⩾ 7). mRNA was enriched using oligo(dT) magnetic beads from the Illumina Gene Expression Sample Prep Kit (Illumina, San Diego, CA, USA) and then fragmented in NEB fragmentation buffer. cDNA was synthesized using the NEBNext Ultra RNA Library Prep Kit (Illumina). Double-stranded cDNA underwent end repair, addition of 3′ poly(A) tails, and ligation of sequencing adapters, followed by purification with the QiaQuick PCR kit (Qiagen, Hilden, Germany). AMPure XP beads were used to select cDNA fragments about 250–300 bp in length, which were then amplified by PCR. The resulting library was purified again with AMPure XP beads, diluted to 1.5 ng·μL^{-1}, and initially quantified using a Qubit 2.0 Fluorometer (Thermo Fisher). Insert sizes were evaluated with the Agilent 2100 Bioanalyzer to ensure they met expectations, and library concentration was precisely measured by RT-qPCR, confirming values above 2 nmol·L^{-1}. Sequencing was performed on a NovaSeq 6000 platform (Illumina) at Beijing Nuohe Zhiyuan Technology. The raw sequencing data are available in the NCBI database under accession number PRJNA1001589.

Raw sequencing data were generated using the CASAVA base-calling software, which transformed the raw sequences into readable sequence data (reads). The quality of these raw reads was evaluated with FastQC, and reads containing splice sites, duplicates, or low sequencing quality were filtered out (specifically, reads with an N ratio exceeding 5% or with more than 20% of bases having a quality score of Q ⩽ 10). Clean reads were then rapidly and accurately aligned to the reference genome using HISAT2 (v2.2.1), a high-performance RNA-seq aligner developed by Kim Laboratory, which provided their genomic positions. Differentially expressed genes (DEGs) were identified using DESeq2, applying criteria of log2 (fold change) ⩾ 1.5 and an adjusted *p*-value ⩽ 0.05. Finally, Gene Ontology (GO) functional analysis and Kyoto Encyclopedia of Genes and Genomes (KEGG) pathway enrichment were conducted using the ClusterProfiler software (v4.0; YuLab SMU) obtained through Bioconductor.

2.4.3 Proteome analysis

The same batch of *N. benthamiana* used for transcriptome analysis was also used to extract total plant proteins[23]. The leaves were ground into powder using liquid nitrogen and then extracted at 25 °C for 2 h in a sucrose lysis buffer containing 0.7 mol·L^{-1} sucrose, 10 mmol·L^{-1} dithiothreitol (DTT), 0.5 mol·L^{-1} Tris-HCl (pH 7), 50 mmol·L^{-1} disodium EDTA, 30 mmol·L^{-1} HCl and 0.1 mol·L^{-1} KCl. An equal volume of tris-phenol was added, and the mixture was shaken for 30 min, then centrifuged at 12,000 *g* and 4 °C for 20 min. The supernatant was collected and mixed with five times its volume of 100% ammonium acetate in methanol (0.1 mol·L^{-1}), then incubated at –20 °C overnight. After centrifugation under the same conditions, the pellet was collected and washed three times, first with methanol containing DTT, then with prechilled acetone containing DTT, before being freeze-dried for over 3 h to obtain total protein samples. The proteins were then ground and dissolved in 8 mol·L^{-1} urea containing 10 mmol·L^{-1} DTT and 0.1 mol·L^{-1} Tris-HCl (pH 8.5), followed by incubation in a metal bath at 37 °C for 1 h. Protein concentration was determined using the Bradford assay[23]. A 400 μg aliquot of total protein was mixed with an equal volume of 50 mmol·L^{-1} ammonium bicarbonate and 55 mmol·L^{-1} iodoacetamide solution, then incubated in the dark at 25 °C for 1 h. The mixture was transferred to a 3 kDa ultrafiltration device and centrifuged at 12,000 *g* and 4 °C for 20 min. After washing with 50 mmol·L^{-1} urea, the sample underwent three additional centrifugation steps with mass spectrometry-grade water. The resulting protein solution, less than 25 μL in volume, was combined with pancreatic enzyme at a 1:20 ratio and digested overnight at 37 °C. Following centrifugation at 12,000 *g* and 4 °C for 20 min, the supernatant was transferred to a 10 kDa ultrafiltration device, mixed with 0.1% formic acid, and centrifuged again under the same conditions. The filtrate was collected and dried to yield the protein samples. Finally, the protein was reconstituted in 0.1% formic acid, transferred to a 200 μL centrifuge tube, and centrifuged at 12,000 *g* and 4 °C for 20 min. The supernatant was then collected for subsequent proteomic analysis.

Total protein was quantified using a TripleTOF 5600 mass spectrometer (SCIEX, Foster City, CA, USA) coupled with the NanoLC415 system (Eksigent, Dublin, CA, USA) and a ChromXP Trap Column (SCIEX; 3 μm C18-CL, 120Å, 350 μm × 0.5 mm). The procedure began with a 10 min demineralization step using buffer A (0.1% formic acid in water) at a flow rate of 2 μL·min^{-1}, followed by a 120 min gradient elution with buffer B (0.1% formic acid in acetonitrile aqueous solution) at 0.3 μL·min^{-1}. The mass spectrometer operated in both positive and negative ion modes, scanning from 350 to 1250 m·z^{-1} with an accumulation time of 200 ms. Secondary mass spectrometry had a scanning range of 100–1500 m·z^{-1} with a 50 ms accumulation time. Ion source

gas 1 was set to 10, ion source gas 2 to 0, and the curtain gas to 35. The ion spray voltage was maintained at 2300 V and the interface heater temperature was set at 150 °C. The proteomics data have been deposited in the ProteomeXchange Consortium database under the data set identifier PXD047688.

Quantitative protein analysis was performed using MaxQuant software (version 1.6.14) developed by the Max Planck Institute of Biochemistry. MS/MS spectra were identified using the Andromeda search engine, referencing PVY protein sequences from UniProt and the tobacco database (Sol Genomics Network, 2025). GO annotations and KEGG pathway information were obtained from the GO database and the KEGG pathway database, respectively. Enrichment analysis of differentially expressed proteins (DEPs) was conducted using hypergeometric testing, comparing proteins with expression changes greater than twofold and a significance threshold of $p < 0.05$.

2.5 Analysis of key genes related to oxidative signal transduction

N. benthamiana plants were treated according to the previously described procedure to assess H_2O_2 levels and defense-related enzyme activities. Leaf samples were collected from the CK, PVY, COS and PVY + COS treatment groups at 1, 3, 5 and 7 days posttreatment, respectively. The expression levels of *MAPKKK21*, *NDPK4* and *MAPK* genes involved in the MAPK signaling pathway, as well as *CAT1*, *SOD*, *POD4*, *GRP1* and *OXI1* genes associated with ROS signal transduction, were measured using RT-qPCR. Gene expression levels were calculated using the $2^{-\Delta\Delta Ct}$ method. Primer sequences for *MAPKKK21*, *NDPK4*, *MAPK*, *CAT1*, *SOD*, *POD4*, *GRP*1 (general receptor for phosphoinositides 1) and *OXI1* used in RT-qPCR are listed in Table S1.

2.6 Western blot analysis of OXI1 protein

Using the aforementioned transcriptome analysis method, *N. benthamiana* plants were treated with PVY alone and with PVY combined with COS. Leaf samples were collected for Western blot analysis at 3 and 5 days posttreatment, respectively. Total proteins were extracted following the protocol outlined in the earlier proteome analysis. The extracted proteins were dissolved in a Tris-HCl buffer containing Tween-20 (TBST), mixed with loading buffer at a 4:1 ratio, and denatured at 100 °C for 10 min. The samples were then separated on a 12% SDS-PAGE gel using a Bio-Rad reagent kit (Bio-Rad, Hercules, CA, USA) at voltages ranging from 80 to 150 V. The gel was imaged using a UV imaging system and cut to isolate the target protein bands. Proteins were transferred from the gel onto a polyvinylidene fluoride membrane via a semidry transfer method, applying a constant voltage of 2.5 V for 7 min with rotation. The membrane was placed in an antibody incubation box and washed three times with TBST at 25 °C. This was then blocked with 5% skimmed milk solution at 25 °C for 1 h, followed by three additional TBST washes. Primary antibodies against *OXI1* (Orizymes, Shanghai, China) and β-actin (ABclona, Wuhan, Hubei, China) were added separately and incubated overnight at 4 °C. After washing with TBST, the membrane was incubated with a secondary antibody (Sangon, Shanghai, China) at 25 °C for 2 h. Following final washes with TBST, chemiluminescent reagents A and B (Sangon, Shanghai, China) were applied for imaging and photography using the UV imaging system.

2.7 *OXI1* biological function assay

This experiment was conducted on wild-type, *OXI1*-overexpressing and *OXI1*-RNAi *N. benthamiana* plants, divided into nine treatment groups: wild-type control (WCK), wild-type with PVY (WPVY), wild-type with PVY and COS (WPCOS), *OXI1*-overexpressing control (OCK), *OXI1*-overexpressing with PVY (OPVY), *OXI1*-overexpressing with PVY and COS (OPCOS), *OXI1*-RNAi control (ICK), *OXI1*-RNAi with PVY (IPVY), and *OXI1*-RNAi with PVY and COS (IPCOS). Each group included three replicates, with 10 plants per replicate. After 24 h of treatment with a 100 μg·mL^{-1} COS solution, the plants were inoculated with PVY using the emery friction inoculation method and with PVY-GFP via *Agrobacterium* infection, respectively. All treated plants were grown in a greenhouse maintained at 26 °C and 70% relative humidity. Five days posttreatment, the expression levels of the MAPKKK*21* and NDPK*4* genes were assessed using RT-qPCR (see Supplementary Information). On day 14 following treatment, anti-PVY phenotypes were evaluated, and the relative expression of the PVY-CP gene was measured by RT-qPCR.

2.8 Data analysis

The data was reported in this study presented as mean values ± standard deviation and was analyzed using GraphPad Prism software (San Diego, CA, USA).

3 Results and analysis

3.1 Protective effect of COS on PVY

As illustrated in Fig. 1, after 14 days of treatment, the application of 100 μg·mL^{-1} COS had strong protective effects against PVY, achieving 54.7% protection, which surpassed the protection provided by CS (40.7%). The resistance phenotype to PVY (Fig. S3) indicates that the leaf number and plant height in PVY + COS-treated plants were greater than those of plants treated with PVY alone after 14 and 28 days of treatment. This indicates that although COS treatment cannot completely inhibit PVY invasion, it can significantly reduce the damage caused by PVY to plants.

3.2 Defense-related enzyme activities and COS-induced H_2O_2 accumulation

Defense-related enzymes are crucial for enabling plants to resist pathogen infections[24]. As shown in Fig. 2(a), on the first day after treatment, the CAT activity in the PVY + COS group reached 189 U·mg^{-1} protein. Although CAT activity decreased from day 1 to day 7, it remained 1.46 times higher than that in the PVY group on day 7. Figure 2(b) shows that the PVY + COS group also had the highest SOD activity on day 1, reaching 15.1 U·mg^{-1} protein. This activity gradually declined over the following 7 days but remained 1.06 times greater than that of the PVY group on day 7. On day 5, POD activity in the PVY + COS group peaked at 2750 U·mg^{-1} protein (Fig. 2(c)). By day 7, POD activity had decreased in all treatments; however, the PVY + COS group still had activity 1.47 times higher than the PVY group. Similarly, on day 5 posttreatment, PAL activity in the PVY + COS group was the highest at 18.0 U·mg^{-1} protein (Fig. 2(d)). Although PAL activity declined by day 7, it remained 1.15 times higher than in the PVY group. Overall, from day 1 to day 7, COS significantly enhanced the activities of defense-related enzymes, with the highest total activity observed on day 5.

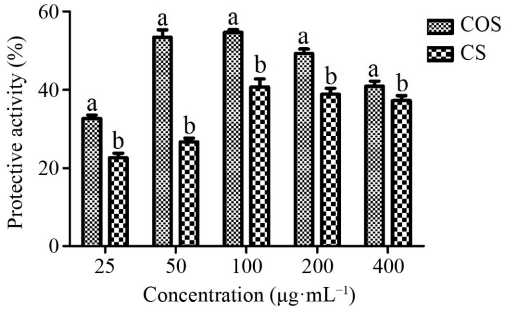

Fig. 1 The protective activity against potato virus Y (PVY) of oligochitosan (COS) and chitosan (CS). Error bars represent the standard error of the mean calculated from three independent experiments. Means with the different letters are significantly different as determined by Student's *t*-test ($p < 0.05$) when compared to the CS group.

H_2O_2 is an essential secondary signaling molecule in plant responses to both abiotic and biotic environmental stresses[25]. As shown in Fig. 2(e), the highest H_2O_2 level was detected on day 1 in the COS group, reaching 1.61 times than that of the CK group. On day 1, the H_2O_2 level in the PVY + COS group peaked at 2.9 μmol·L^{-1}·g^{-1} FW, which was 1.38 times higher than that in the PVY group alone. These results indicate that COS significantly induces an increase in H_2O_2 levels in *N. benthamiana*. Also, Fig. S4 indicates that COS can trigger bursts of superoxide anions and NO in *N. benthamiana*, and exerts a protective effect on tobacco leaf cells, further supporting the role of COS in inducing ROS bursts.

3.3 Transcriptome analysis

As shown in Table S2, the quality of the sequencing data meets the requirements for transcriptome analysis. The Venn diagram in Fig. 3(a) shows that 34,398 genes were identified in the PVY + COS group, while 34,072 genes were identified in the PVY group. Of these, 32,718 genes were common to both treatments, with 1680 DEGs identified in the PVY + COS group and 1354 DEGs in the PVY group. The volcano plot in Fig. 3(b) reveals that, compared to the PVY treatment, a total of 730 genes (marked by red dots) were upregulated and 436 genes (marked by green dots) downregulated following PVY + COS treatment. All DEGs from the transcriptome analysis of PVY and PVY + COS are listed in Table S3. Functional annotation of DEGs was performed using GO terms with Table S4 presenting enrichment of 258 biological process (BP) terms, 40 cellular component (CC) terms, and 220 molecular function (MF) terms. The top 10 terms in each BP, CC, and MF category are displayed in Fig. 3(c). Notably, seven DEGs are enriched in the BP category related to defense response and are associated with plant disease resistance. To further explore the role of plant immune signal transduction in COS, KEGG analysis was conducted on DEGs, revealing a total of 91 co-enriched KEGG pathways (Table S5). Figure 3(d) shows the top 20 KEGG pathways, highlighting that five upregulated DEGs are

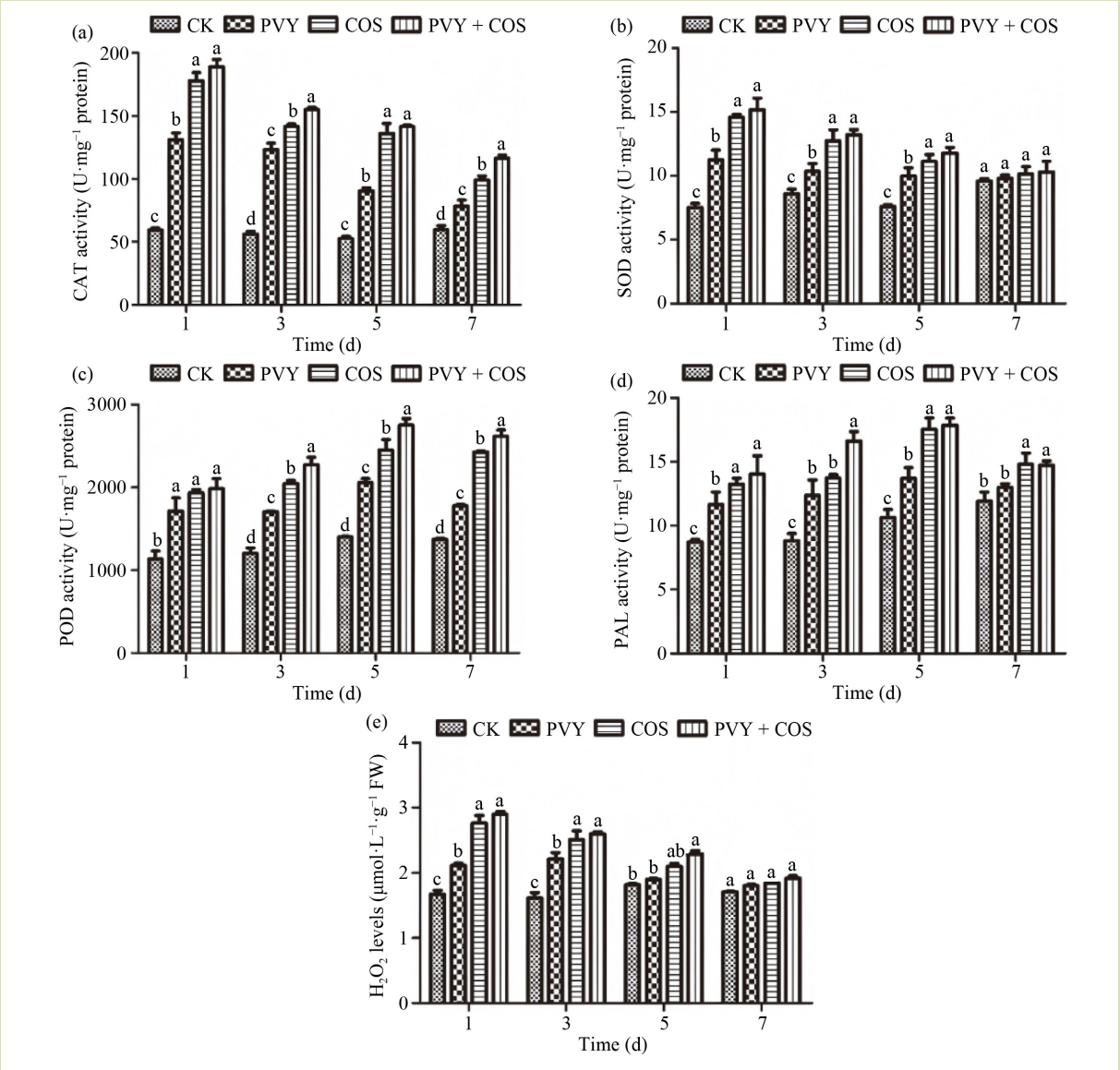

Fig. 2 (a) Aatalase (CAT), (b) superoxide dismutase (SOD), (c) peroxidase (POD) and (d) phenylalanine ammonia-lyase (PAL) activity in *Nicotiana benthamiana* leaves treated with oligochitosan (COS) and potato virus Y (PVY). (e) Hydrogen peroxide level in *N. benthamiana* leaves treated with COS and PVY. Error bars represent the standard error of the mean calculated from three independent experiments. Means with the different letters are significantly different as determined by Student's *t*-test ($p < 0.05$) when compared to the control group (CK) group.

associated with the MAPK signaling pathway (nta04016), seven DEGs are involved in the plant hormone signaling pathway (nta04075), and six DEGs are linked to the plant-pathogen interaction pathway (nta04626). These GO and KEGG analysis results indicate that COS may stimulate the expression of disease resistance genes in *N. benthamiana*.

3.4 Proteome analysis

Quantitative analysis of protein content in *N. benthamiana* leaves was performed using the iBAQ algorithm. As illustrated by the Venn diagram (Fig. 4(a)), a total of 1090 proteins were identified across the PVY and PVY + COS treatment groups, with 977 proteins detected in the PVY group and 944 in the

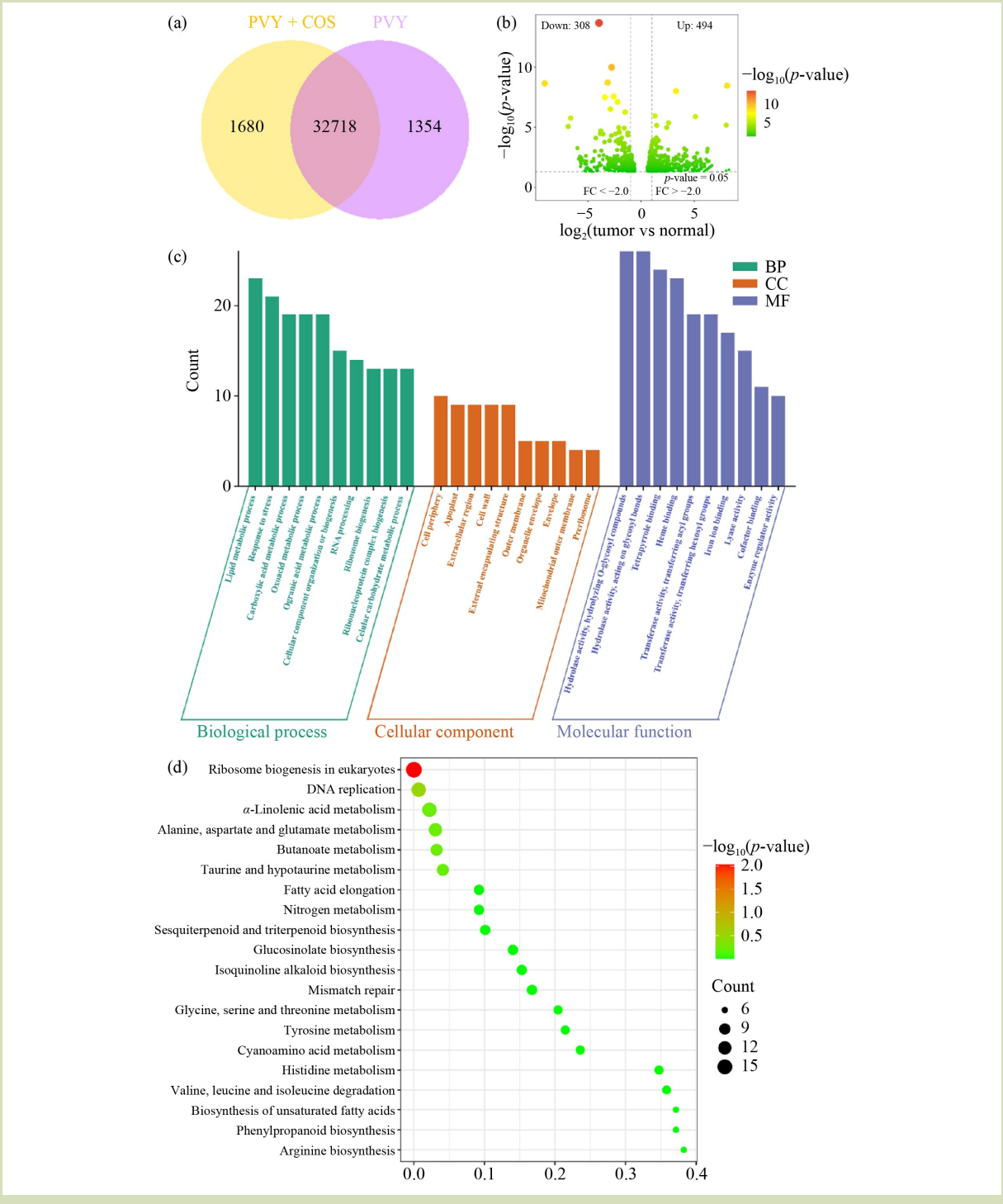

Fig. 3 Transcriptome analysis of *Nicotiana benthamiana* in potato virus Y (PVY) plus oligochitosan (COS) vs PVY treatment. (a) Venn diagram for genes identified in different treatments. (b) Volcano plot of differentially expressed genes (DEGs) in the two treatments. Red dots represent upregulated genes, and green dots represent downregulated genes. (c) Gene Ontology (Go) term enrichment analysis of DEGs in two different treatments. (d) Top 20 Kyoto Encyclopedia of Genes and Genomes (KEGG) pathways enrichment of DEGs in the two treatments.

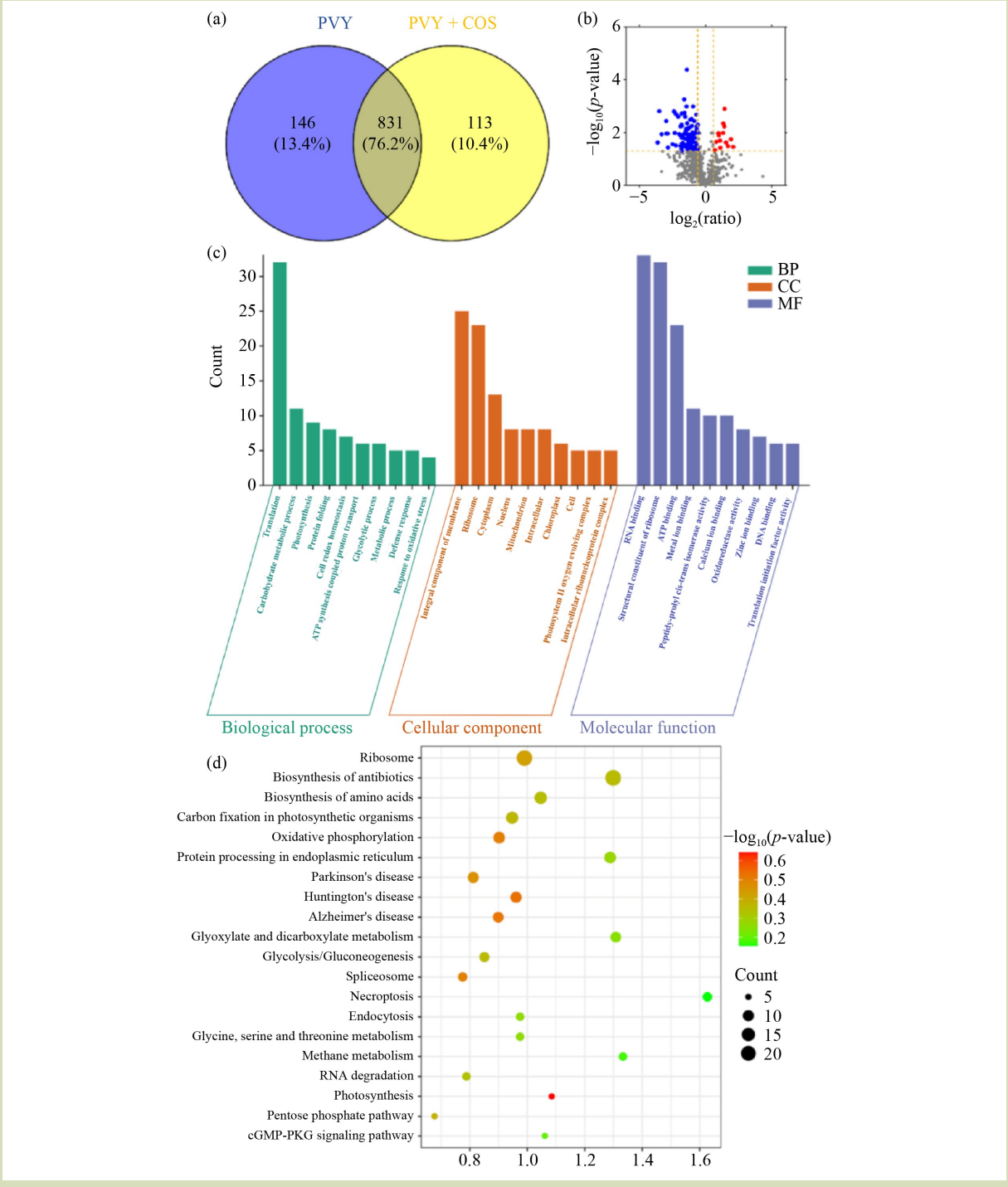

Fig. 4 Proteome analysis of *Nicotiana benthamiana* in potato virus Y (PVY) plus oligochitosan (COS) vs PVY treatment. (a) Venn diagram for genes identified in the treatments. (b) Volcano plot of differentially expressed genes (DEGs) in the two treatments. Red dots represent upregulated genes, and green dots represent downregulated genes. (c) Gene Ontology (Go) enrichment analysis of DEGs in the two treatments. (d) Top 20 Kyoto Encyclopedia of Genes and Genomes (KEGG) pathways enrichment of DEGs in the two treatments.

PVY + COS group. Of these proteins, 13.4% had differential expression in response to PVY infection, while 10.4% showed differential expression following PVY + COS treatment (Table S6). The volcano plot (Fig. 4(b)) indicates that, compared to the PVY group, the PVY + COS group displayed 14 upregulated proteins (red dots) and 106 downregulated proteins (blue dots). GO analysis was performed to characterize the functions of the DEPs, with 77, 232, and 170 DEPs enriched in CC, MF and BP, respectively (Table S7). The leading GO terms within each category are shown in Fig. 4(c). Notably, 14 DEPs within the molecular function category were associated with defense responses, implicating their involvement in plant disease resistance. Concurrently, KEGG pathway analysis identified enrichment of DEPs across 226 pathways (Table S8). Pathways enriched with more than 10 DEPs are presented in Fig. 4(d), highlighting the MAPK signaling pathway, which contributes to plant immune responses, and was enriched with 10 DEPs, as well as the plant-pathogen interaction pathway enriched with eight DEPs. Collectively, the GO and KEGG analyses indicate that COS induces the expression of proteins associated with disease resistance in *N. benthamiana*.

3.5 Combined analysis of the transcriptome and proteome

3.5.1 Analysis of the correlation expression of differentially expressed genes

Transcriptome sequencing data were used to predict coding sequences and derive the corresponding protein sequences for database searches. DEPs identified through proteome analysis were considered as proteins involved in both translational and transcriptional processes, with their corresponding genes designated as related genes. A total of 33 genes having expression at both transcriptional and translational levels are presented in Table S9. Of these, 13 genes were upregulated, six genes were downregulated, and 14 genes displayed divergent expression patterns between the two levels. Notably, genes such as *USP*, *HSP*70 and *POD4*, which showed consistent upregulation at both transcriptional and translational stages, are known to be involved in plant stress responses and disease resistance. Additionally, cellulose synthase-like *H1*, *NDPK4* and *NtCaM10* were also upregulated and are associated with plant cell wall biosynthesis, activation of the MAPK signaling pathway and Ca^{2+}-mediated cellular signaling, respectively.

3.5.2 Functional correlation analysis of KEGG pathways

Transcriptomic and proteomic data sets were simultaneously annotated using the KEGG database. Sixty-seven KEGG pathways were identified, revealing annotation overlap between DEPs and DEGs, resulting in a combined enrichment of 295 DEGs and 169 DEPs. Figure 5(a) illustrates the principal KEGG pathways jointly annotated with more than 10 DEGs and DEPs. The top three KEGG pathways having the highest enrichment of DEGs and DEPs were oxidative phosphorylation (ko:00190), biosynthesis of amino acids (ko:01230), and carbon fixation in photosynthetic organisms (ko:00710), all of which are involved in fundamental material and energy metabolism in plants. Notably, pathways related to plant hormone signal transduction (ko:04075), plant-pathogen interaction (ko:04626) and the MAPK signaling pathway in plants (ko:04016) were also identified, each critical in the signal transduction mechanisms underlying plant disease resistance.

The genes Niben101Scf02085 g21007 (LOC107816664, *PYL*1) and Niben101Scf00611 g08002 (LOC107776835, *PP2C*) were found to be enriched within the plant hormone signal transduction pathway, specifically annotated to the abscisic acid (ABA) signaling cascade. The core components of the ABA receptor-mediated signaling pathway include PYR1, PYL9, PP2C and SnRK2[26]. Under external stress, plants synthesize or release ABA, which subsequently binds to PYR/PYL receptors to form receptor-ligand complexes. These complexes inhibit PP2C phosphatases, thereby releasing SnRK2 from PP2C-mediated repression. Activated SnRK2 then phosphorylates downstream transcription factors, leading to the activation of the ABA signaling pathway[27]. Transcriptomic analyses demonstrated that treatment with COS results in the upregulation of PYR1 expression and the downregulation of PP2C expression. Based on these findings, it is proposed that COS modulates the ABA signaling pathway, thereby enhancing plant resistance to PVY.

The DEGs and DEGs enriched within the plant-pathogen interaction pathway (ko:04626) were predominantly associated with the calcium (Ca^{2+}) signaling pathway. Notably, the identified DEPs include Q76MF3_TOBAC (LOC107761764, NtCaM3), A0A1S3ZDE0_TOBAC (LOC107785602, HSP90-5), A0A1S4AFF5_TOBAC (LOC107796888, CML13), Q76ME6_TOBAC (LOC107779518, NtCaM10) and Q76MF4_TOBAC (LOC107781984, NtCaM2). Correspondingly, the DEGs comprised Niben101Scf02824 g03017 (LOC107813448, CML41), Niben101Scf15327 g00001 (LOC107792571, CML),

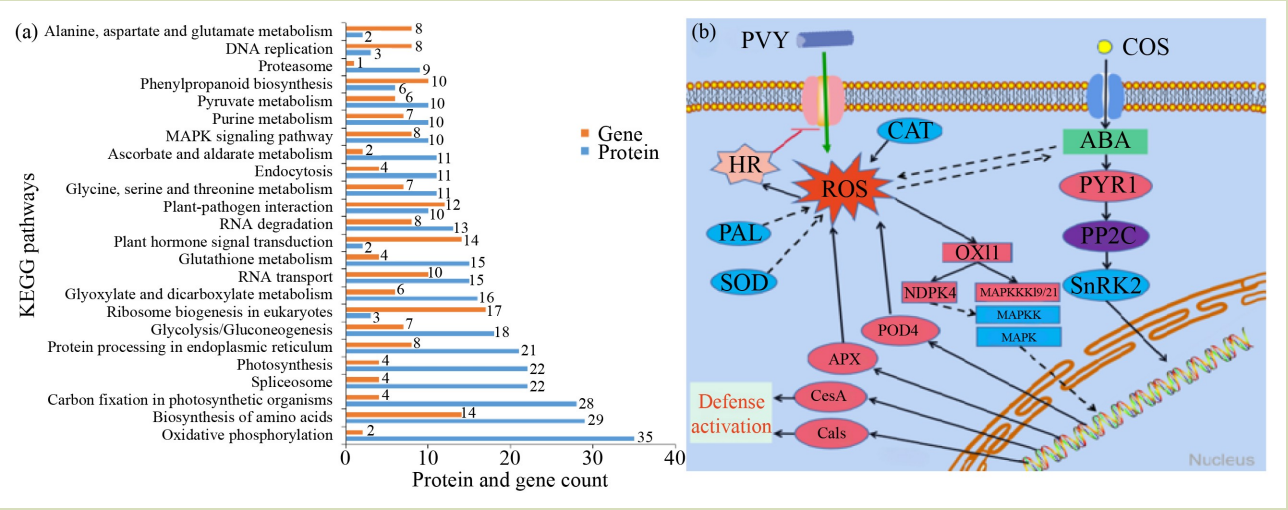

Fig. 5 (a) Kyoto Encyclopedia of Genes and Genomes (KEGG) pathways co-annotated by transcriptome and proteome of *Nicotiana benthamiana* in potato virus Y (PVY) plus oligochitosan (COS) vs PVY treatment. (b) The signaling transduction pathway of COS-induced against PVY in *N. benthamiana*. The red module indicates a significant upregulation of related genes and the purple module represents a significant downregulation. The blue module indicates that the relevant genes were not significantly upregulated or detected.

and Niben101Scf03049 g00001 (LOC107807848, HSP82). Given the extensive enrichment of multiple Ca^{2+}-related genes within the plant-pathogen interaction pathway, which are commonly implicated in plant-pathogen infection processes, this KEGG pathway and its associated genes were not prioritized for further investigation.

On binding to the membrane receptor, the downstream protein GRP1 interacts with inositol 3-phosphate, thereby modulating oxidative signaling and the MAPK signal transduction pathway[28]. OXI1 functions as a pivotal kinase linking ROS to multiple downstream signaling cascades and serves as a critical activator of the MAPK signaling pathway[29]. Also, OXI1 is essential for the activation of MAPK3 and MAPK6 and influences the expression of NDPK2[30]. NDPK facilitates the transfer of phosphate groups between nucleoside diphosphates and nucleoside triphosphates, thereby promoting the expression of genes involved in plant cell signal transduction and defense mechanisms[31]. Integrated transcriptomic and proteomic analyses demonstrated that COS induces the upregulation of *OXI1*, *MAPKKK21*/*19* and *NDPK4* expression. Complementary physiologic and biochemical assessments revealed that COS triggers H_2O_2 bursts and requires Ca^{2+} influx to elicit resistance against PVY in *N. benthamiana*. Collectively, these findings indicate that COS stimulates ROS signaling, which is subsequently transmitted intracellularly via the MAPK pathway.

The DEPs enriched within the MAPK signaling pathway (ko:04016) included A0A1S4BFY9_TOBAC (LOC107807832, *PR-1B*), Q76MF3_TOBAC (*NtCaM3*), A0A1S3Z1Y6_TOBAC (LOC107782115, *NDPK4*), Q76ME6_TOBAC (LOC107779518, *NtCaM9*) and Q76MF4_TOBAC (LOC107781984, *NtCaM9*). Correspondingly, the DEGs associated with this pathway comprised Niben101Scf05152 g00001 (LOC107789122, *OXI1*), Niben101Scf02407 g04002 (LOC107782115, *NDPK4*), Niben101Scf06715 g02006 (LOC107776219, *MAPKKK21*), Niben101Scf00168 g10008 (LOC107817780, *MAPKKK*19) and Niben101Scf00063 g10026 (LOC107779518, *CaM10*). Notably, these genes showed enrichment in the MAPK signaling pathway in both transcriptomic and proteomic data sets. Therefore, this study focused on elucidating the effects of COS on the MAPK signaling cascade in plants, with particular emphasis on its upstream and downstream regulatory components.

POD and APX are critical in plants by scavenging excess H_2O_2 and other peroxides, thereby maintaining ROS homeostasis and significantly contributing to the induction of plant disease resistance[32]. Callose, a polysaccharide integral to plant

defense against pathogen invasion, is synthesized by the enzyme callose synthase (Cals), which is essential for the adaptive response of plants to external stressors[33]. Additionally, cell wall thickening represents a primary defense mechanism against plant diseases, with cellulose synthase (CesA) serving as a key enzyme in cellulose biosynthesis, thereby reinforcing the cell wall structure[34]. Consequently, the upregulation of functional proteins such as POD4, APX, Cals and CesA by COS, coupled with enhanced defense-related enzymatic activities and cell wall fortification, constitutes a pivotal mechanism through which COS mediates resistance to PVY.

In summary, COS predominantly modulates MAPK and ABA signaling pathways, leading to the induction of callose, cellulose and defense enzyme expression in *N. benthamiana*, thereby mitigating PVY-induced damage. A preliminary model of the underlying signal transduction pathway is proposed in Fig. 5(b). It is postulated that COS interacts with specific receptors on the cell membrane, initiating a cascade in which COS promotes the accumulation of ROS, including H_2O_2, which subsequently activates the expression of *OXI1*. OXI1 then facilitates the phosphorylation of NDPK4 and upregulates MAPKKK19 and MAPKKK21, thereby propagating and amplifying immune signaling via the MAPK cascade. This signaling cascade ultimately induces the expression of *Cals-5*, *POD* and *APX*, orchestrating a defensive response against PVY infection.

3.6 COS-induced expression of key genes in ROS signaling transduction and MAPK signaling pathways

G protein-coupled receptors are localized on the plant cell membrane and are important for recognizing extracellular signals[27]. Previous studies have also identified the presence of COS receptors on cell membranes[7]. As illustrated in Fig. 6(a), the expression of the *GRP1* gene in the PVY + COS treatment group peaked on the third day posttreatment, showing increases of 1.46-fold and 5.3-fold relative to the PVY and CK treatments, respectively. These findings indicate that COS induces the upregulation of the *GRP*1 gene. OXI1, a key regulator of ROS bursts and plant PTI, had a similar expression pattern. As shown in Fig. 6(b), the expression level of the *OXI1* gene in the PVY + COS treatment reached its maximum on day 3, with increases of 1.55-fold and 5.84-fold compared to PVY and CK treatments, respectively, followed by a gradual decline on days 5 and 7. This indicates that COS promotes the upregulation of genes involved in oxidative signal transduction in *N. benthamiana*. Also, studies in *Arabidopsis* have confirmed that OXI1 positively regulates the expression of downstream genes such as *MAPKKK* and *NDPK*2.

As illustrated in Fig. 6(c), COS exerts the most pronounced effect on the expression of *MAPKKK21*. On day 3 following treatment with PVY combined with COS, the expression level of *MAPKKK21* peaked, reaching 1.9-fold that observed under PVY treatment alone. Concurrently, the expression of the *MAPK* gene also reached its maximum level on the same day, having a 1.46-fold increase relative to PVY treatment (Fig. 6(d)). Also, by day 5, as shown in Fig. 6(e), the expression of the *NDPK4* gene reached its highest point under PVY + COS treatment, showing a 1.39-fold elevation compared to PVY treatment alone. These findings indicate that COS induces the upregulation of key genes within the MAPK signaling pathway in *N. benthamiana*.

As shown in Fig. 6(f), *CAT1* peaked on day 1 after PVY + COS treatment, having a 1.53-fold increase compared to PVY treatment alone, before gradually declining thereafter. The expression level of the *POD4* gene progressively increased from day 1 to day 5, reaching its maximum on day 5, which was 1.34 times higher than that observed under PVY treatment (Fig. 6(g)). Similarly, *SOD* gene expression reached its highest level 3 days posttreatment, representing a 1.36-fold increase relative to PVY treatment (Fig. 6(h)). These findings indicate that COS treatment significantly enhances the expression of peroxisome-related genes in *N. benthamiana*. This observation corroborates previous analyses demonstrating increased defense enzyme activity, elevated H_2O_2 content, and the upregulation of the *POD4* gene identified through transcriptomic and proteomic studies.

3.7 COS-induced OXI1 protein production

OXI1 serves as a pivotal component in plant ROS signal transduction and the activation of downstream immune pathways[29]. To further investigate the translational expression of OXI1, Western blot analysis was performed, with the results presented in Fig. 7. After 3 and 5 days of treatment, OXI1 accumulation was significantly higher in the PVY + COS treatment group compared to the PVY-only group. Additionally, OXI1 expression levels were greater in the 100 μg·mL^{-1} COS treatment than in the 50 μg·mL^{-1} COS treatment. These findings corroborate the influence of COS on OXI1 expression at the protein level.

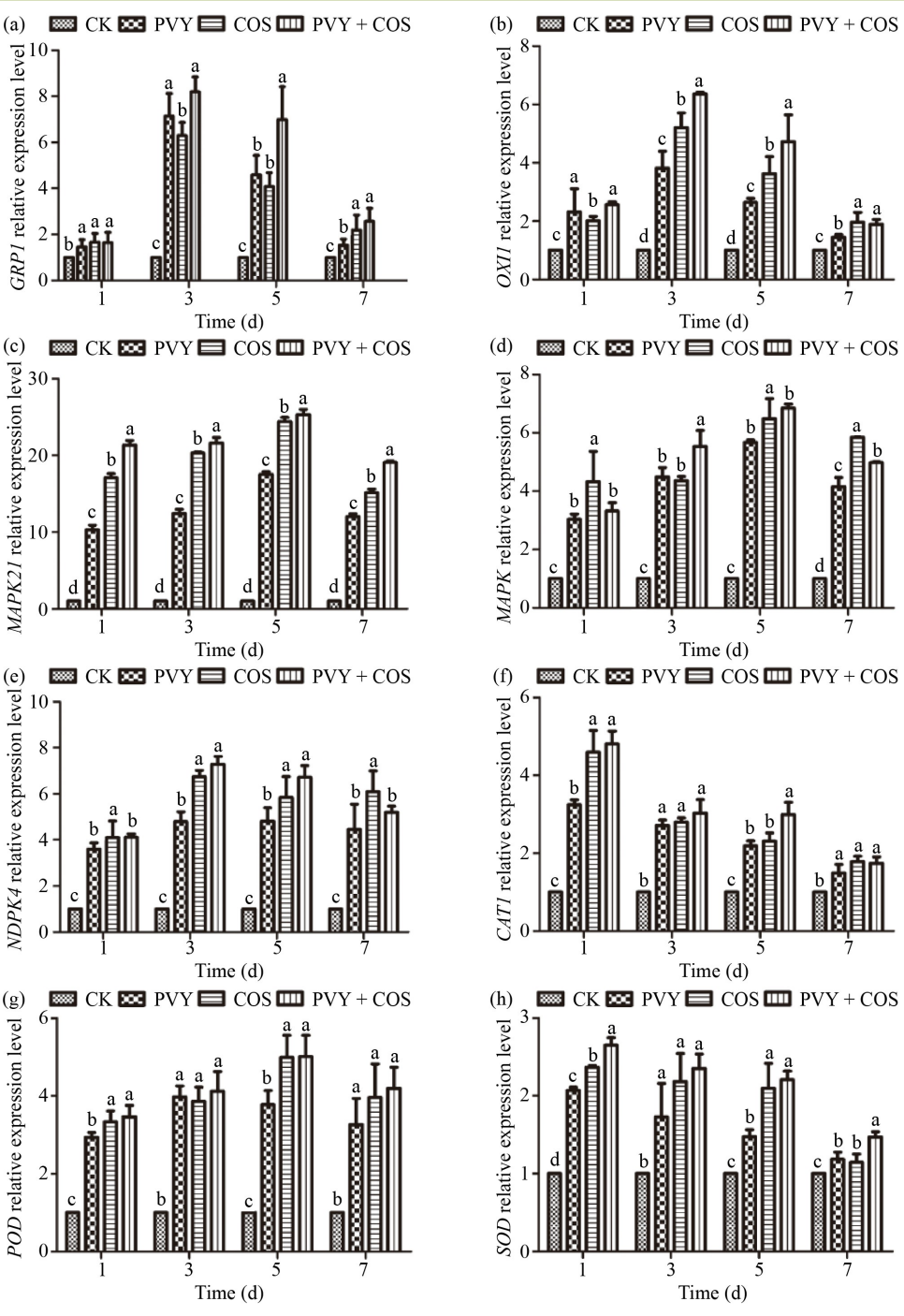

Fig. 6 Oligochitosan (COS)-induced the relative expression levels of general receptor for (a) phosphoinositides 1 (*GRP1*), (b) oxidative stress inducible type 1 (*OXI1*), (c) mitogen-activated protein kinase kinase kinase 21 (*MAPKKK21*), (d) mitogen-activated protein kinase (*MAPK*), (e) nucleoside diphosphate kinase 4 (*NDPK4*), (f) catalase 1 (*CAT1*), (g) peroxidase (*POD*) and (h) superoxide dismutase (*SOD*) genes in *Nicotiana benthamiana*. Error bars represent the standard error of the mean calculated from three independent experiments. Means with the different letters are significantly different as determined by Student's *t*-test ($p < 0.05$) when compared to the control group (CK).

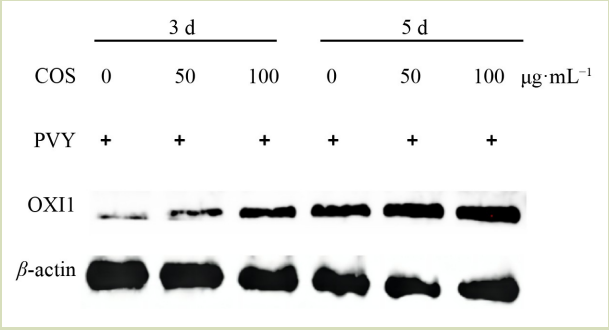

Fig. 7 Photo of Western Blot analysis of oxidative stress inducible type 1 (OXI1) induced by oligochitosan (COS) in *Nicotiana benthamiana.*

3.8 Biological function of *OXI1*-mediated anti-PVY

As shown in Fig. 8(a), after inoculated with PVY using the emery friction method, the upper stems and petioles of plants treated with IPVY significantly turned black and withered. Plants treated with WPVY also withered in the upper regions; however, no stem withering was observed in the petioles, indicating a milder effect compared to IPVY treatment. In contrast, plants treated with OPVY displayed only shrinkage symptoms in the heart leaves without any evident wilting. These findings indicate that *OXI1* significantly enhances plant resistance to PVY infection.

To further elucidate the role of the *OXI1* gene in conferring resistance to PVY, an activity assay was conducted using *OXI1* mutant plants inoculated with PVY-GFP via *Agrobacterium*-mediated infection. As shown in Fig. 8(b), after 14 days of treatment, plants subjected to the IPVY treatment had dwarfism, pronounced wrinkling of the heart leaves, and widespread green fluorescence under UV light, indicative of PVY-GFP infection, compared to the WCK. The relative increase in PVY-CP levels in IPVY plants was the highest, reaching 112%, whereas the IPCOS treatment showed a comparatively lower increase of 71%. Conversely, plants in the OPVY group displayed markedly milder symptoms,

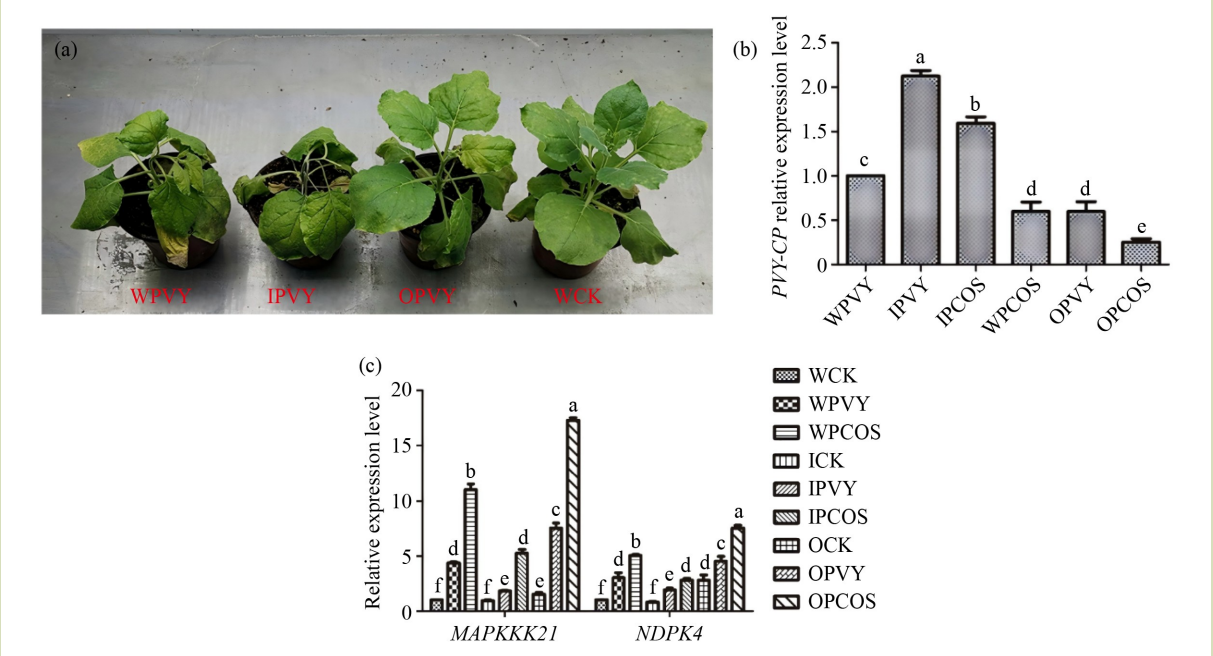

Fig. 8 Biological function of Oxidative stress inducible type 1 (*OXI1*)-mediated anti potato virus Y (PVY) in *Nicotiana benthamiana.* (a) Phenotype of the *OXI1* mutants resistance to PVY. (b) Expression level of PVY coat protein (*PVY-CP*) gene in the *OXI1* mutants. (c) Expression level of mitogen-activated protein kinase kinase kinase 21 (*MAPKKK21*) and Nucleoside Diphosphate Kinase 4 (*NDPK4*) in the *OXI1* mutants. Error bars represent the standard error of the mean calculated from three independent experiments. Means with the different letters are significantly different as determined by Student's *t*-test ($p < 0.05$) when compared to the control group.

characterized by reduced green fluorescence and a greater number of leaves. Correspondingly, PVY-CP expression in OPVY plants was significantly decreased by 40%, with the OPCOS treatment having the most substantial reduction of 75%. These findings indicate that *OXI1* functions as a positive regulator in COS-induced resistance against PVY infection.

As demonstrated in Fig. 8(c), the expression level of *MAPKKK21* in the OPVY treatment was 7.2-fold higher compared to the WCK control. In the WPVY and IPVY treatments, *MAPKKK21* expression was increased by 3.8-fold and 1.7-fold relative to WCK, respectively. Additionally, MAPKKK*21* expression in the OPCOS treatment was 4.29 times greater than in WPVY, while in IPCOS it was 1.2 times higher than in WPVY. These findings indicate that *OXI1* positively regulates *MAPKKK21* expression in *N. benthamiana*, and that COS treatment simultaneously induces upregulation of both *OXI1* and *MAPKKK21*. Also, as shown in Fig. 8(c), among the three CK treatments, the relative expression of *NDPK4* was highest in the OCK group, having a 2.8-fold increase compared to WCK, whereas expression in the ICK group was only 0.8 times that of WCK. Notably, *NDPK4* expression following OPCOS treatment was 2.5 times higher than in WPVY and 2.68 times greater than in IPCOS. The data indicate that *OXI1* positively influences *NDPK4* expression, as evidenced by increased *NDPK4* levels in *OXI1*-overexpressing plants and decreased levels in *OXI1*-RNAi lines. COS treatment concurrently promotes the upregulation of both *OXI1* and *NDPK4* in *N. benthamiana*. Collectively, these results indicate that COS-induced *OXI1* exerts a positive regulatory effect on plant resistance to PVY by modulating the expression of *MAPKKK21* and *NDPK4* within the downstream MAP kinase signaling pathway. Consequently, this study further substantiates that COS mediates the MAPK pathway via ROS signaling, thereby influencing both PTI and ETI to enhance plant resistance against PVY infection.

4 Discussion

COS function as biological inducers of plant immunity, demonstrating significant efficacy against a range of phytopathogenic fungi, bacteria, and viruses[3]. The present study reveals that COS concentrations between 50 and 100 μg·mL^{-1} elicit an anti-PVY response in *N. benthamiana* exceeding 50%. Also, treatment with 100 μg·mL^{-1} COS enhances the activities of defense-related enzymes, including *CAT*, *POD*, *PAL*, and *SOD*, concomitant with the induction of ROS accumulation. These findings indicate that COS effectively induces resistance in *N. benthamiana* against PVY infection, corroborating prior research outcomes.

Transcriptomic and proteomic analyses revealed that COS modulate the differential expression of critical genes in *N. benthamiana*, including *OXI1*, *NDPK4*, *MAPKKK21*, *MAPKKK19*, *POD4*, *APX*, *CesA*, *Cals*, *PYR1* and *PP2C*. These genes are involved in oxidative signaling and are significantly enriched within the MAPK signaling pathway. Notably, MAPKKK and MAPK serve as pivotal components of the plant MAPK signaling cascade, while *GRP1*, *OXI1* and *NDPK4* are crucial for regulating oxidative signaling processes in plants[13,17,31]. Subsequent RT-qPCR analyses demonstrated that COS treatment upregulated the expression of MAPK pathway genes (*MAPKKK21* and *MAPK*), peroxisomal genes (*CAT1*, *SOD*, *POD* and *PAL1*), and oxidative signal transduction genes (*GRP1*, *OXI1* and *NDPK4*) in *N. benthamiana*. Concurrently, Western blot assays confirmed that COS induced increased protein levels of OXI1 and NDPK4. The activation of the oxidative signaling pathway represents an early plant response to elicitor-induced disease resistance and functions upstream of the MAPK signaling pathway[35]. OXI1 is recognized as a central component within the plant oxidative signaling network[13]. Functional assays involving *OXI1* mutants revealed that overexpression of *OXI1* enhances *N. benthamiana* resistance to PVY, whereas silencing of *OXI1* reduces this resistance. Also, *OXI1* positively regulates downstream genes *MAPKKK21* and *NDPK4*, with COS treatment promoting upregulation of *OXI1* expression. Collectively, these findings indicate that COS induce *OXI1* expression in *N. benthamiana*, thereby modulating MAPK signal transduction. Consequently, COS mediate MAPK pathway activation through ROS signaling to confer antiviral effects against PVY in *N. benthamiana*.

5 Conclusions

This study demonstrates that COS confers resistance to PVY in *N. benthamiana* by enhancing the activity of defense-related enzymes and promoting H_2O_2 accumulation. Integrative multi-omics analyses identified that COS treatment upregulates KEGGs involved in ABA, MAPK, and oxidative signaling pathways, specifically *PYL1*, *PP2C*, *OXI1*, *NDPK4*, *MAPKKK21* and *POD4*. Subsequent validations showed that COS induces the overexpression of *OXI1*, *MAPKKK21* and *NDPK4* through

ROS-mediated MAPK signaling cascades. Also, functional studies using *OXI1* mutants confirmed the essential role of OXI1 in mediating PVY resistance. Collectively, these findings identify ROS-dependent MAPK activation as the central mechanism underlying COS-induced antiviral defense responses in *N. benthamiana*.

Supplementary materials

The online version of this article at https://doi.org/10.15302/J-FASE-2025666 contains supplementary materials (Figs. S1–S4; Tables S1–S9).

Acknowledgements

The authors acknowledge financial support from the National Key Research and Development Program of China (2023YFD1700505).

Compliance with ethics guidelines

Shanxue Zhang, Chunle Wei, Lu Yu, and Baoan Song declare that they have no conflicts of interest or financial conflicts to disclose. This article does not contain any studies with human or animal subjects performed by any of the authors.

REFERENCES

1. Qiu D, Dong Y, Zhang Y, Li S, Shi F. Plant immunity inducer development and application. *Molecular Plant-Microbe Interactions*, 2017, **30**(5): 355–360
2. Liu Y, Yang H, Wen F, Bao L, Zhao Z, Zhong Z. Chitooligosaccharide-induced plant stress resistance. *Carbohydrate Polymers*, 2023, **302**: 120344
3. Yin H, Du Y, Dong Z. Chitin oligosaccharide and chitosan oligosaccharide: two similar but different plant elicitors. *Frontiers in Plant Science*, 2016, **7**: 522
4. Deng Y Y, Ming J, Zhang Z Q, Zeng K F. Effect of chitosan on salicylic acid and active oxygen metabolism of navel orange fruit. *Scientia Agricultura Sinica*, 2010, **43**(4): 812–820 (in Chinese)
5. Quenouille J, Vassilakos N, Moury B. Potato virus Y: a major crop pathogen that has provided major insights into the evolution of viral pathogenicity. *Molecular Plant Pathology*, 2013, **14**(5): 439–452
6. Shibuya N, Minami E. Oligosaccharide signalling for defence responses in plant. *Physiological and Molecular Plant Pathology*, 2001, **59**(5): 223–233
7. Liu D, Jiao S, Cheng G, Li X, Pei Z, Pei Y, Yin H, Du Y. Identification of chitosan oligosaccharides binding proteins from the plasma membrane of wheat leaf cell. *International Journal of Biological Macromolecules*, 2018, **111**: 1083–1090
8. Zhu F, Xi D H, Yuan S, Xu F, Zhang D W, Lin H H. Salicylic acid and jasmonic acid are essential for systemic resistance against tobacco mosaic virus in *Nicotiana benthamiana*. *Molecular Plant-Microbe Interactions*, 2014, **27**(6): 567–577
9. Yin H, Zhao X, Bai X, Du Y. Molecular cloning and characterization of a *Brassica napus* L. MAP kinase involved in oligochitosan-induced defense signaling. *Plant Molecular Biology Reporter*, 2010, **28**(2): 292–301
10. Chen Z, Silva H, Klessig D F. Active oxygen species in the induction of plant systemic acquired resistance by salicylic acid. *Science*, 1993, **262**(5141): 1883–1886
11. Torres M A, Jones J D G, Dangl J L. Reactive oxygen species signaling in response to pathogens. *Plant Physiology*, 2006, **141**(2): 373–378
12. Levine A, Tenhaken R, Dixon R, Lamb C. H_2O_2 from the oxidative burst orchestrates the plant hypersensitive disease resistance response. *Cell*, 1994, **79**(4): 583–593
13. Shoala T, Edwards M G, Knight M R, Gatehouse A M R. OXI1 kinase plays a key role in resistance of *Arabidopsis* towards aphids (*Myzus persicae*). *Transgenic Research*, 2018, **27**(4): 355–366
14. Majeed Y, Zhu X, Zhang N, Rasheed A, Tahir M M, Si H. Functional analysis of mitogen-activated protein kinases (MAPKs) in potato under biotic and abiotic stress. *Molecular Breeding*, 2022, **42**(6): 31
15. Liang Y J, Yang W X. Kinesins in MAPK cascade: how kinesin motors are involved in the MAPK pathway. *Gene*, 2019, **684**: 1–9
16. Bigeard J, Hirt H. Nuclear signaling of plant MAPKs. *Frontiers in Plant Science*, 2018, **9**: 469
17. Dorion S, Rivoal J. Clues to the functions of plant NDPK isoforms. *Naunyn-Schmiedeberg's Archives of Pharmacology*, 2015, **388**(2): 119–132
18. Lee D G, Ahsan N, Lee S H, Kang K Y, Lee J J, Lee B H. An

approach to identify cold-induced low-abundant proteins in rice leaf. *Comptes Rendus Biologies*, 2007, **330**(3): 215–225

19. Ishikawa T, Morimoto Y, Madhusudhan R, Sawa Y, Shibata H, Yabuta Y, Nishizawa A, Shigeoka S. Acclimation to diverse environmental stresses caused by a suppression of cytosolic ascorbate peroxidase in tobacco BY-2 cells. *Plant & Cell Physiology*, 2005, **46**(8): 1264–1271
20. Valenti D, Vacca R A, de Pinto M C, De Gara L, Marra E, Passarella S. In the early phase of programmed cell death in Tobacco Bright Yellow 2 cells the mitochondrial adenine nucleotide translocator, adenylate kinase and nucleoside diphosphate kinase are impaired in a reactive oxygen species-dependent manner. *Biochimica et Biophysica Acta - Bioenergetics*, 2007, **1767**(1): 66–78
21. Matsushita Y, Suzuki T, Kubota R, Mori M, Shimosato H, Watanabe M, Kayano T, Nishio T, Nyunoya H. Isolation of a cDNA for a nucleoside diphosphate kinase capable of phosphorylating the kinase domain of the self-incompatibility factor SRK of *Brassica* campestris. *Journal of Experimental Botany*, 2002, **53**(369): 765–767
22. Yuan M, Jiang Z, Bi G, Nomura K, Liu M, Wang Y, Cai B, Zhou J M, He S Y, Xin X F. Pattern-recognition receptors are required for NLR-mediated plant immunity. *Nature*, 2021, **592**(7852): 105–109
23. Zhang J, Zhao L, Zhu C, Wu Z, Zhang G, Gan X, Liu D, Pan J, Hu D, Song B. Facile synthesis of novel vanillin derivatives incorporating a bis(2-hydroxyethyl)dithhioacetal moiety as antiviral agents. *Journal of Agricultural and Food Chemistry*, 2017, **65**(23): 4582–4588
24. Pirzadah T B, Malik B, Tahir I, Rehman R U, Hakeem K R, Alharby H F. Aluminium stress modulates the osmolytes and enzyme defense system in *Fagopyrum* species. *Plant Physiology and Biochemistry*, 2019, **144**: 178–186
25. Niu L, Liao W. Hydrogen peroxide signaling in plant development and abiotic responses: crosstalk with nitric oxide and calcium. *Frontiers in Plant Science*, 2016, **7**: 230
26. Lin Z, Li Y, Wang Y, Liu X, Ma L, Zhang Z, Mu C, Zhang Y, Peng L, Xie S, Song C P, Shi H, Zhu J K, Wang P. Initiation and amplification of SnRK2 activation in abscisic acid signaling. *Nature Communications*, 2021, **12**(1): 2456
27. García-Andrade J, González B, Gonzalez-Guzman M, Rodriguez P L, Vera P. The role of ABA in plant immunity is mediated through the PYR1 receptor. *International Journal of Molecular Sciences*, 2020, **21**(16): 5852
28. Neer E J. Heterotrimeric C proteins: organizers of transmembrane signals. *Cell*, 1995, **80**(2): 249–257
29. Rentel M C, Lecourieux D, Ouaked F, Usher S L, Petersen L, Okamoto H, Knight H, Peck S C, Grierson C S, Hirt H, Knight M R. OXI1 kinase is necessary for oxidative burst-mediated signalling in *Arabidopsis*. *Nature*, 2004, **427**(6977): 85810.1094/MPMI-11-13-0349-R861
30. Mishra N S, Tuteja R, Tuteja N. Signaling through MAP kinase networks in plants. *Archives of Biochemistry and Biophysics*, 2006, **452**(1): 55–68
31. Ye J, Ding W, Chen Y, Zhu X, Sun J, Zheng W, Zhang B, Zhu S. A nucleoside diphosphate kinase gene OsNDPK4 is involved in root development and defense responses in rice (*Oryza sativa* L.). *Planta*, 2020, **251**(4): 77
32. Moustafa-Farag M, Mohamed H I, Mahmoud A, Elkelish A, Misra A N, Guy K M, Kamran M, Ai S, Zhang M. Salicylic acid stimulates antioxidant defense and osmolyte metabolism to alleviate oxidative stress in watermelons under excess boron. *Plants*, 2020, **9**(6): 724
33. Li N, Lin Z, Yu P, Zeng Y, Du S, Huang L J. The multifarious role of callose and callose synthase in plant development and environment interactions. *Frontiers in Plant Science*, 2023, **14**: 1183402
34. Eckardt N A. Cellulose synthesis takes the *CesA* train. *Plant Cell*, 2003, **15**(8): 1685–1687
35. Pitzschke A, Djamei A, Bitton F, Hirt H. A major role of the MEKK1–MKK1/2–MPK4 pathway in ROS signalling. *Molecular Plant*, 2009, **2**(1): 120–137